Article

Theoretical Determination of High-Energy Photon Attenuation and Recommended Protective Filler Contents for Flexible and Enhanced Dimensionally Stable Wood/NR and NR Composites

Worawat Poltabtim [1], **Donruedee Toyen** [2] **and Kiadtisak Saenboonruang** [1,3,*]

[1] Department of Applied Radiation and Isotopes, Faculty of Science, Kasetsart University, Bangkok 10900, Thailand; wp.worawat@gmail.com
[2] Scientific Equipment and Research Division, Kasetsart University Research and Development Institute (KURDI), Kasetsart University, Bangkok 10900, Thailand; rdiddt@ku.ac.th
[3] Specialized Center of Rubber and Polymer Materials in Agriculture and Industry (RPM), Faculty of Science, Kasetsart University, Bangkok 10900, Thailand
[*] Correspondence: kiadtisak.s@ku.th; Tel.: +662-562-5555 (ext. 1217)

Abstract: This work aimed to theoretically determine the high-energy-photon-shielding properties of flexible wood/natural rubber (NR) and NR composites containing photon protective fillers, namely Pb, Bi_2O_3, or Bi_2S_3, using XCOM. The properties investigated were the mass attenuation coefficient (μ_m), linear attenuation coefficient (μ), and half value layer (HVL) of the composites, determined at varying photon energies of 0.001–5 MeV and varying filler contents of 0–1000 parts per hundred parts of rubber by weight (phr). The simulated results, which were in good agreement with previously reported experimental values (average difference was 5.3%), indicated that overall shielding properties increased with increasing filler contents but decreased with increasing incident photon energies. The results implied the potential of bismuth compounds, especially Bi_2O_3, to replace effective but highly toxic Pb as a safer high-energy-photon protective filler, evidenced by just a slight reduction in μ_m values compared with Pb fillers at the same filler content and photon energy. Furthermore, the results suggested that the addition of 20 phr wood particles, primarily aimed to enhance the rigidity and dimensional stability of Pb/NR, Bi_2O_3/NR, and Bi_2S_3/NR composites, did not greatly reduce shielding abilities; hence, they could be used as dimensional reinforcers for NR composites. Lastly, this work also reported the optimum Pb, Bi_2O_3, or Bi_2S_3 contents in NR and wood/NR composites at photon energies of 0.1, 0.5, 1, and 5 MeV, with 316–624 phr of filler being the recommended contents, of which the values depended on filler type and photon energy of interest.

Keywords: natural rubber; wood particles; Bi_2O_3; Bi_2S_3; Pb; photon; gamma; X-ray; shielding; XCOM

1. Introduction

High-energy photons, especially X-rays and gamma rays, are presently used in various applications, for instance, X-ray and gamma imaging for medical and industrial purposes [1–3], radiotherapy for cancer treatment [4], gamma irradiation on plants for mutation breeding [5], and X-ray fluorescence (XRF) for elemental analysis [6]. However, despite their benefits and potentials, excessive exposure to high-energy photons could fatally harm users and the general public [7], with the symptoms including skin burn, loss of appetite, nausea, vomiting, abdominal pain, fever, diarrhea, loss of hair, damage to bone marrow, cancer, and even death [8–10]. Herein, a radiation safety principle called "As Low As Reasonably Achievable" or "ALARA" must be strictly followed in all radiation- and nuclear-related facilities [11].

One of the three ALARA principles is the use of effective and appropriate radiation-shielding equipment that could sufficiently reduce radiation exposure on users to within occupational dose limits recommended by the International Commission on Radiological

Protection (ICRP) [12]. However, as technologies relying on the use of high-energy photons are rapidly expanded, development in novel and better radiation-shielding equipment is constantly pursued with specific added-on properties such as flexibility, transparency, environmental friendliness, and self-healing ability. Examples of newly developed high-energy photon-shielding materials are self-healing gamma-shielding hydrogels from nano-bismuth oxide (nano-Bi_2O_3)/poly(vinyl) alcohol (PVA) [10], flexible ethylene propylene diene monomer (EPDM) and natural rubber (NR) composites containing metal oxides [13,14], biocompatible polyaniline reinforced with hybrid graphene oxide-iron tungsten nitride flakes [15], and environmental-friendly Bi_2O_3-filled concrete [16].

Among these materials used for the production of radiation-shielding equipment, NR has presented itself as one of the most interesting materials due to excellent tensile properties, high tear resistance, lower odor than synthetic rubber (SR), and waterproofing ability [17]. However, pristine NR is not readily the most effective shielding materials as NR mostly consists of light elements that have low interaction probabilities with high-energy photons. As a result, appropriate fillers must be incorporated into the NR matrix to increase the probability of interactions. Specifically for X-ray and gamma rays, it has been known and widely accepted that heavy metals and heavy-metal-containing compounds, especially involving lead (Pb), are generally used as economical and effective protective fillers due to their high atomic numbers (Z) and densities (ρ), which could increase interactions between materials and incident photons through the mechanisms of the photoelectric absorption, Compton scattering, and pair production that consequently result in better radiation attenuation [18,19]. In addition, Pb is also economically accessible such that low-cost shielding materials could be produced [20]. However, despite its advantages, Pb is highly toxic and hazardous to humans, animals, plants, and the environment as it could damage the brain and blood systems of living organisms, causing abdominal pain, constipation, headaches, irritability, and even death [21]. Therefore, alternative heavy-metal-containing compounds such as bismuth compounds, especially Bi_2O_3 and Bi_2S_3, which are considered safer for producers and users than Pb, has gained much attention from researchers [13,14]. For example, the report from Poltabtim et al. showed that EPDM composites containing 500 phr Bi_2O_3 had a linear attenuation coefficient (μ) of 24.3 ± 2.2 m^{-1} at a gamma energy of 1.25 MeV [13], which was comparable with NR composites containing the same Pb content that had a μ value of 26.0 m^{-1} [22]. This comparison implied the high potential of Bi_2O_3 and Bi_2S_3 to replace Pb as effective and safe protective fillers.

Although high contents of Bi_2O_3 and Bi_2S_3 in NR composites generally resulted in enhanced shielding properties, the overall mechanical properties of the composites could be inversely reduced, mostly due to their poor interfacial compatibility and the different contraction/expansion behaviors during curing and cooling processes between NR and Bi_2O_3 (Bi_2S_3), which possibly created voids between the surfaces of the two substances. Furthermore, high filler contents could also lead to agglomerations of particles from filler-filler interactions. Consequently, these effects lowered the overall strength and flexibility of the materials. Examples of the effects from high filler contents are a decrease in the tensile strength of Bi_2O_3/NR composites from ~13 MPa in a sample with 100-phr Bi_2O_3 to ~8 MPa and ~6 MPa for samples with 300-phr and 500-phr Bi_2O_3, respectively [13]. Thus, the effects of radiation protective fillers in improving shielding properties but also lowering the overall mechanical properties of the composites are two competing factors which researchers and product developers must pay close attention to in order to produce NR composites that are effective, safe, and usable for all the intended applications.

In addition to the filler contents that could affect the shielding and mechanical properties of NR composites, the self-solid-lubricant properties of most metal compounds added to NR could result in decreased crosslink densities, shortened lifetimes, and unpleasantly expanded dimensions of the NR composites after some periods of usage [23]. For instance, Ninyong et al. reported that the dimensions of 80-phr B_2O_3/NR composites, which were developed as flexible neutron shielding materials, increased by 44% after normal usage at room temperature for 150 days. Subsequently, this unfortunate behavior led to a signif-

icant reduction in the shielding abilities of the material (approximately 36%) due to the decrease in material thickness by 31% that resulted in lower photon interactions with the materials [24]. To enhance dimensional stability of the NR composites, fillers with high rigidity and roughness such as wood particles could be used by incorporating them into NR composites. This improvement in dimensional stability after the addition of wood particles was also confirmed by Ninyong et al., who showed that by adding 20 phr of wood particles into NR composites, the dimension of 80-phr B_2O_3/NR composites increased by just 14% after 150 days of usage, resulting in a decrease in the shielding abilities by 13% compared to the 36% drop in those without the addition of wood particles [24]. Clearly, the wood particles showed potential to be used as a dimensional reinforcer in Bi_2O_3/NR and Bi_2S_3/NR composites, especially in the case of high filler contents.

Consequently, the current work aimed to theoretically determine the high-energy photon shielding properties, based on the mass attenuation coefficient (μ_m), linear attenuation coefficient (μ), and half value layer (*HVL*) of Pb/NR, Bi_2O_3/NR, and Bi_2S_3/NR composites with or without the addition of wood particles using XCOM provided by the National Institute of Standards and Technology (NIST) [25]. To fully understand effects of filler contents and photon energies on shielding properties, the Pb and Bi_2O_3 contents as well as the photon energy used in the simulation were varied in the ranges 0–1,000 phr and 0.001–5 MeV, respectively, and the obtained results were compared with previously reported experimental values with similar material preparations and testing procedures to ensure the correctness and the reliability of the simulated results. Furthermore, the investigation reported and discussed the recommended filler contents of Pb, Bi_2O_3, and Bi_2S_3 in wood/NR and NR composites at various gamma energies (0.1 MeV, 0.5 keV, 1 MeV, and 5 MeV), which were selected based on the determination of the least filler content that increased the μ value of the composites by less than 5% after the addition of 40 phr of the filler. This content optimization was carried out to minimize the negative effects on the mechanical properties of the composites from high filler contents while still offering relatively high shielding ability.

2. Simulation Setup and Determination of High-Energy Photon Shielding Properties

2.1. Simulation Setup

The web-based XCOM software provided by the National Institute of Standards and Technology (NIST), Gaithersburg, MD, USA, was used to determine the values of μ_m in the wood/NR and NR composites containing Bi_2O_3, Bi_2S_3, or Pb particles (μ_m represent the fraction of attenuated incident photons in a monoenergetic beam per unit mass) [25]. Originally, the XCOM software was developed to ease tedious and complicated numerical calculation of photon cross sections for compounds, especially at the absorption edges, which was usually carried out by finding weighted sums of individual cross sections for all of the atomic constituents. Furthermore, cross sections at energies immediately above and below all absorption edges, which have discontinuous photo-absorption cross sections that lead to complications in usual numerical calculation, are automatically included in XCOM. The photon cross section database used in this work was the NIST standard reference database 8 (XGAM), released in November 2010. The contents of the chemicals used for the wood/NR and NR composites were entered as a mixture, with the formulation of the composites shown in Table 1, and the photon energies were entered from 0.001–5 MeV. It should be noted that the values of μ_m reported in this work were calculated from the total attenuation with the inclusion of coherent scattering [26].

Table 1. Name, chemical formula, content, and density of chemicals used for the simulation in this work [14,20].

Chemical	Chemical Formula	Content (phr *)	Density (g/cm³)
Natural rubber (NR)	C_5H_8	100	0.92
Stearic acid	$C_{18}H_{36}O_2$	3	0.94
Zinc oxide	ZnO	5	5.6
Mercaptobenzothiazole (MBT)	$C_7H_5NS_2$	2	1.46
Diphenylguanidine (DPG)	$C_{13}H_{13}N_3$	3	1.19
Carbon black	C	40	1.95
Sulfur	S	4	2.1
Wood particles (cellulose)	$C_6H_{10}O_5$	0 or 20	0.52
Bismuth oxide, bismuth sulfide, or lead	Bi_2O_3, Bi_2S_3 or Pb	0–1000	8.90, 6.78 or 11.35

* phr: parts per hundred parts of rubber by weight.

2.2. Determination of μ and HVL

The values of μ and HVL, which represent the fraction of attenuated incident photons in a monoenergetic beam per unit thickness and the thickness of the materials required to attenuate 50% of incident photons, respectively, of the wood/NR and NR composites containing Bi_2O_3, Bi_2S_3, or Pb particles with contents varying from 0 to 1000 phr at photon energies of 0.001–5 MeV were determined from the obtained values of μ_m (XCOM) using Equations (1) and (2), respectively:

$$\mu = \mu_m \rho \tag{1}$$

$$HVL = \frac{ln(2)}{\mu} \tag{2}$$

where ρ is the density of the composites theoretically estimated using Equation (3):

$$\rho = \frac{\sum_i c_i}{\sum_i \frac{c_i}{\rho_i}} \tag{3}$$

where i is the ith chemical in Table 1, ρ_i is the density of the ith chemical in Table 1, and c_i is the content of the ith chemical in Table 1 [13].

2.3. Determination of Recommended Bi_2O_3, Bi_2S_3, and Pb Contents

The recommended Bi_2O_3, Bi_2S_3, and Pb contents at photon energies of 0.1, 0.5, 1, and 5 MeV were determined by considering the percentage change in μ_m (%*change*) after the addition of 40 phr of fillers and was calculated using Equation (4):

$$\% \ change = \frac{\mu_{m,2} - \mu_{m,1}}{\mu_{m,1}} \tag{4}$$

where $\mu_{m,1}$ is the initial μ_m of the composites and $\mu_{m,2}$ is the resulting μ_m of the composites after the additional 40-phr Bi_2O_3, Bi_2S_3, or Pb.

To obtain the recommended contents for each filler type and photon energy, %*change* for all contents (0–1000 phr) were determined and the least contents that had %*change* less than 5% were selected as the recommended contents (the threshold of %*change*, which was 5% in this work, could be varied depending on users' preferences). Furthermore, in order to determine recommended contents at any photon energies besides the reported values at 0.1, 0.5, 1, and 5 MeV, trendlines were also developed using equations in the form:

$$f(x) = Ax^B \tag{5}$$

where *f(x)* is the threshold of %*change*, *x* is the recommended filler content, and *A* and *B* are mathematical constants determined using a trendline function available in Microsoft Excel. It should be noted that the objective of this determination was to minimize the effects of too-high filler contents on lowering the mechanical properties of the composites.

3. Results and Discussion

3.1. Mass Attenuation Coefficient (μ_m)

The μ_m values at photon energies of 0.001–5 MeV for Bi_2O_3/NR, Bi_2S_3/NR, Pb/NR, Bi_2O_3/wood/NR, Bi_2S_3/wood/NR, and Pb/wood/NR composites with varying filler contents of 0, 400, and 800 phr are shown in Figures 1–4. The results indicated that the composites with the addition of Bi_2O_3, Bi_2S_3, or Pb had noticeably higher μ_m values than the pristine NR and wood/NR composites at all investigated photon energies (Figures 1–3), with the μ_m values increased with increasing filler contents (Figure 4). This could have resulted from the added Bi_2O_3 (Bi_2S_3), which contained Bi atoms, and the Pb particles greatly enhanced the interaction probabilities between the incident photons and the composites through photoelectric absorption, Compton scattering, and pair production (pair production could occur only at photon energies greater than 1.022 MeV) due to their high Z and ρ values, with the relationships between the cross sections for each mechanism and its photon/material characteristics being shown as Equations (6)–(8):

$$\sigma_{pe} \propto \frac{Z^n}{(h\nu)^3} \tag{6}$$

$$\sigma_{comp} \propto \frac{1}{n_e} \tag{7}$$

$$\sigma_{pp} \propto Z^2 \tag{8}$$

where σ_{pe} is the photoelectric cross section, σ_{comp} is the Compton scattering cross section, σ_{pp} is the pair production cross section, Z is the atomic number of the element, h is Planck's constant, ν is the frequency of the photon, and n_e is the electron density, which is related to density and Z of the material [27].
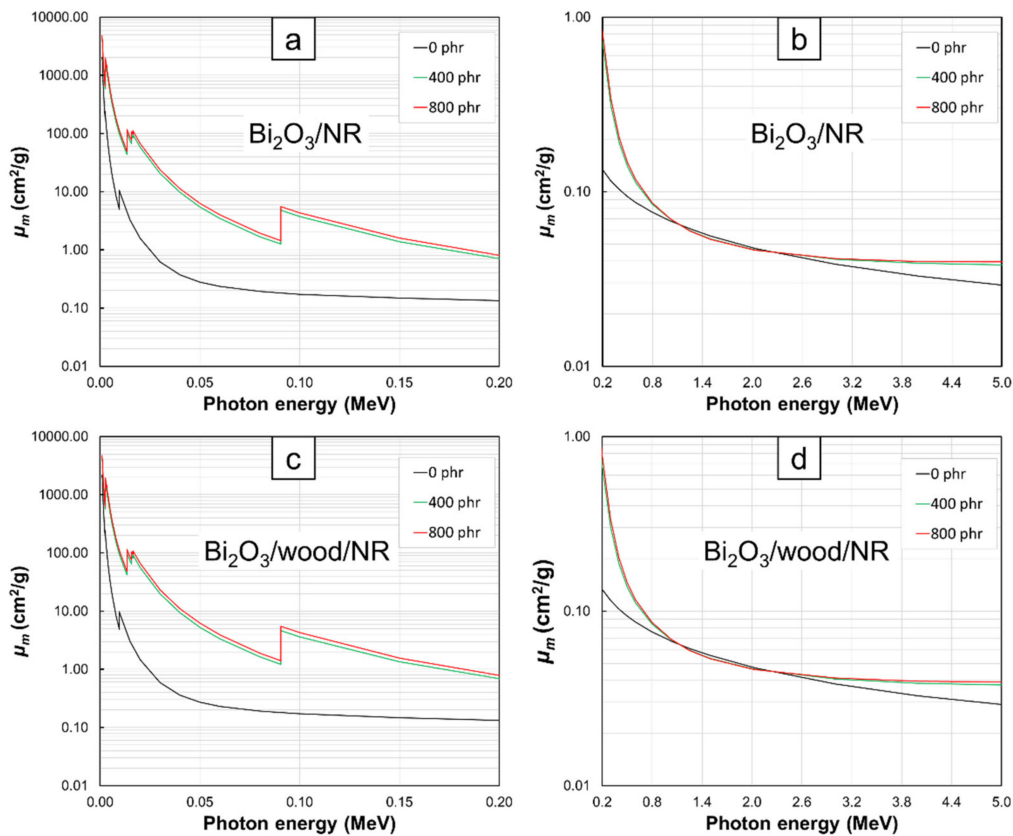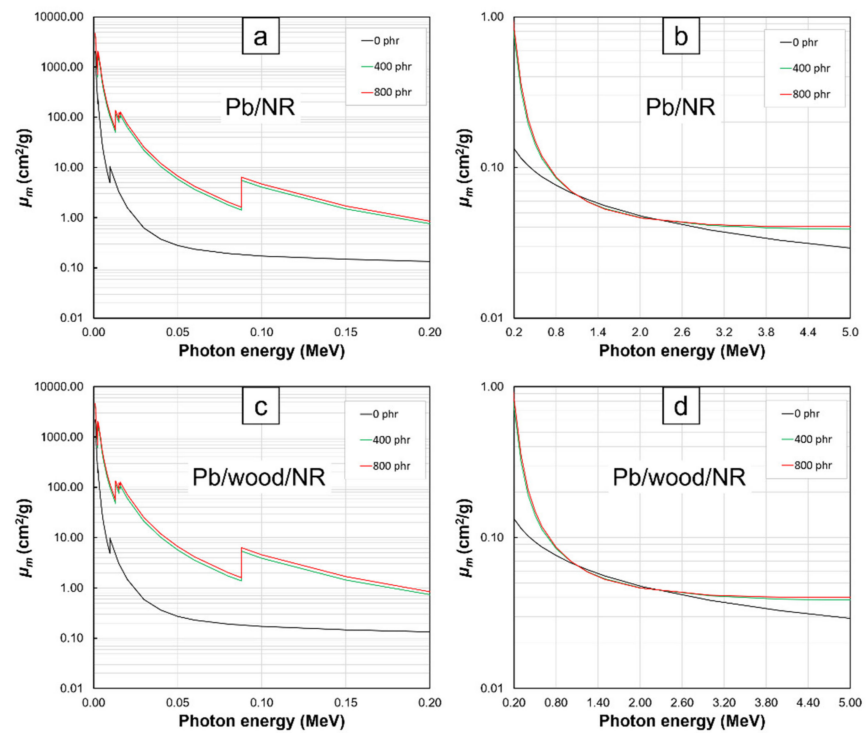

Figure 1. μ_m values of (**a**,**b**) Bi_2O_3/NR and (**c**,**d**) Bi_2O_3/wood/NR composites with filler contents of 0, 400, and 800 phr, determined at photon energies of (**a**,**c**) 0.001–0.2 MeV and (**b**,**d**) 0.2–5 MeV using XCOM. Raw data are provided in the Supplementary Materials (Tables S1, S2, S3, S8, S9, and S10).
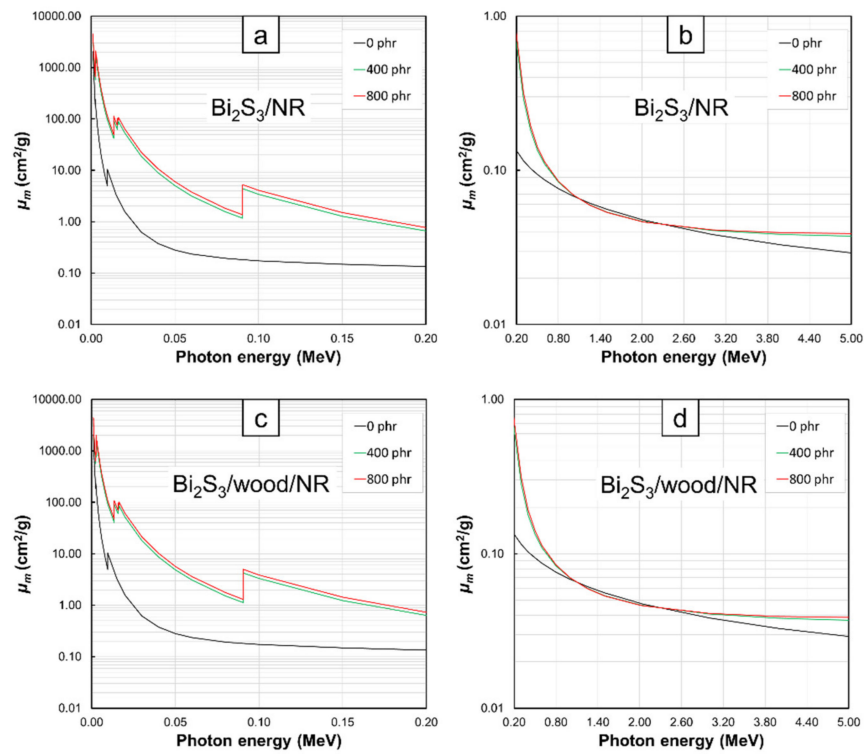
Figure 2. μ_m values of (**a**,**b**) Bi_2S_3/NR and (**c**,**d**) Bi_2S_3/wood/NR composites with filler contents of 0, 400, and 800 phr, determined at photon energies of (**a**,**c**) 0.001–0.2 MeV and (**b**,**d**) 0.2–5 MeV using XCOM. Raw data are provided in the Supplementary Materials (Tables S1, S6, S7, S8, S13, and S14).
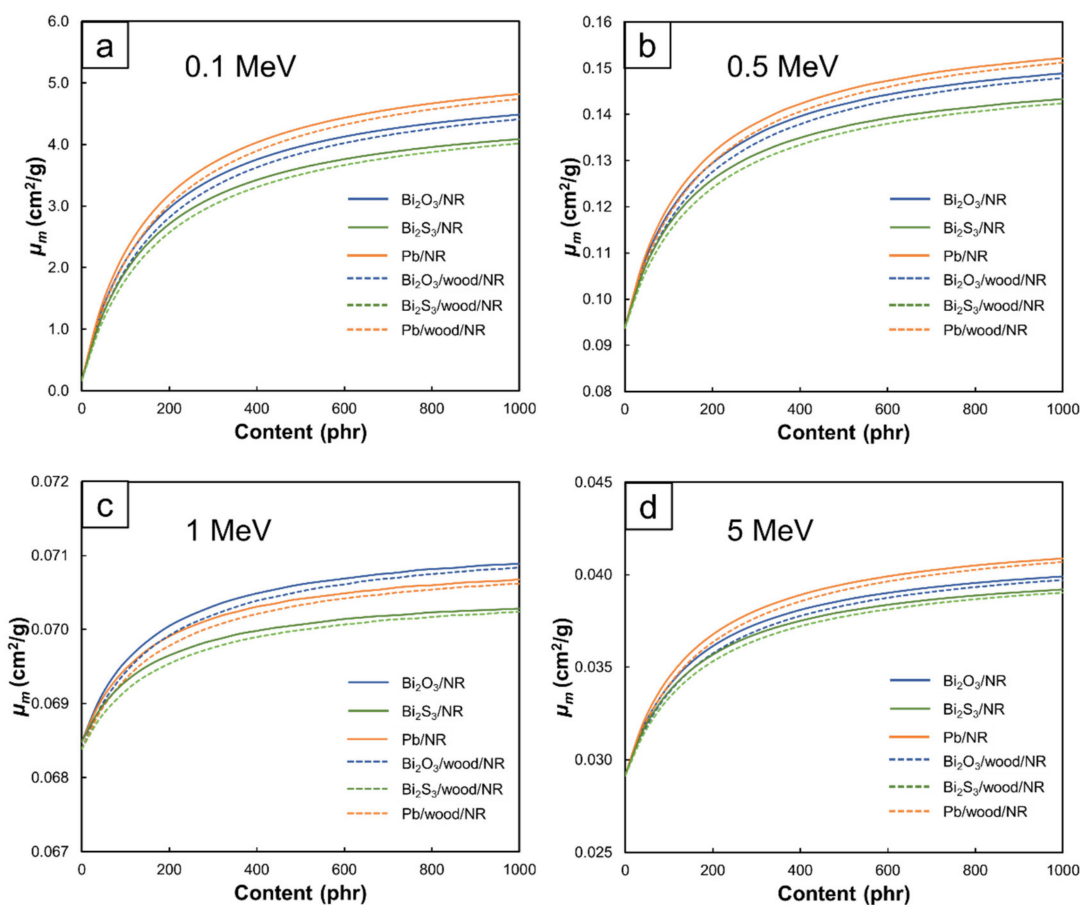

Figure 3. μ_m values of (**a**,**b**) Pb/NR and (**c**,**d**) Pb/wood/NR composites with filler contents of 0, 400, and 800 phr, determined at photon energies of (**a**,**c**) 0.001–0.2 MeV and (**b**,**d**) 0.2–5 MeV using XCOM. Raw data are provided in the Supplementary Materials (Tables S1, S4, S5, S8, S11, and S12).
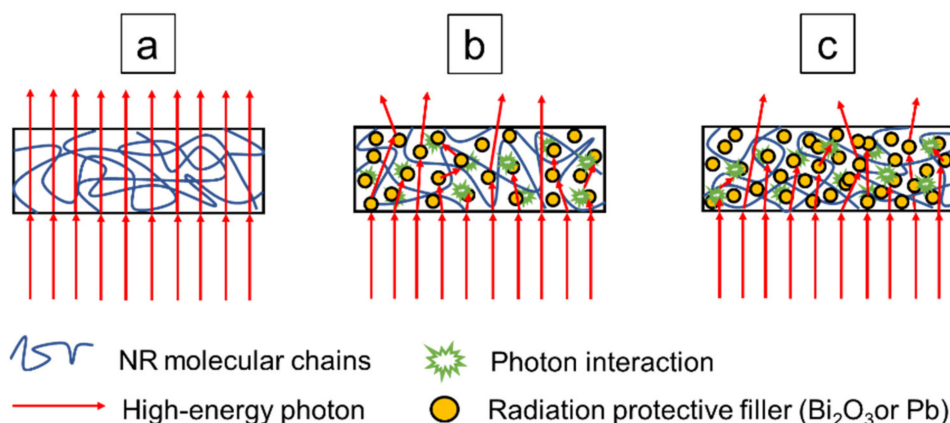
Figure 4. μ_m values of Bi_2O_3/NR, Bi_2O_3/wood/NR, Bi_2S_3/NR, Bi_2S_3/wood/NR, Pb/NR, and Pb/wood/NR composites with filler contents varied from 0–1000 phr, determined at photon energies of (**a**) 0.1 MeV, (**b**) 0.5 MeV, (**c**) 1 MeV, and (**d**) 5 MeV using XCOM.

The effects of Bi_2O_3 and Pb and their contents on enhancing high-energy photon attenuation are graphically illustrated in Figure 5.


Figure 5. Scheme showing interactions of incident photons and NR composites for (**a**) a pristine NR, (**b**) and (**c**) NR composites containing radiation protective fillers (filler contents of (**c**) greater than (**b**)).

Furthermore, the results in Figures 1–3 revealed that μ_m values tended to decrease with increasing photon energies and the effects of fillers on μ_m were more pronounced at lower energies. These behaviors were observed because higher-energy photons were less

likely to interact with materials they encountered than lower-energy photons due to the inverse relationship between linear energy transfer (*LET*) and photon energies [28], leading to less energy loss or absorption and consequently, less photon attenuation and μ_m values. Interestingly, there were sharp increases in the values of μ_m in NR composites containing Bi_2O_3, Bi_2S_3, and Pb at photon energies of:

- 13–16. keV and 90.5 keV in Bi_2O_3/NR, Bi_2S_3/NR, Bi_2O_3/wood/NR, and Bi_2S_3/wood/NR composites (Figure 1a,c and Figure 2a,c) due to the L-edge and K-edge of Bi atoms in Bi_2O_3 and Bi_2S_3, respectively (Figure 6)
- 13–16. keV and 88.0 keV in Pb/NR and Pb/wood/NR composites (Figure 3a,c) due to the L-edge and K-edge of Pb atoms, respectively (Figure 6)
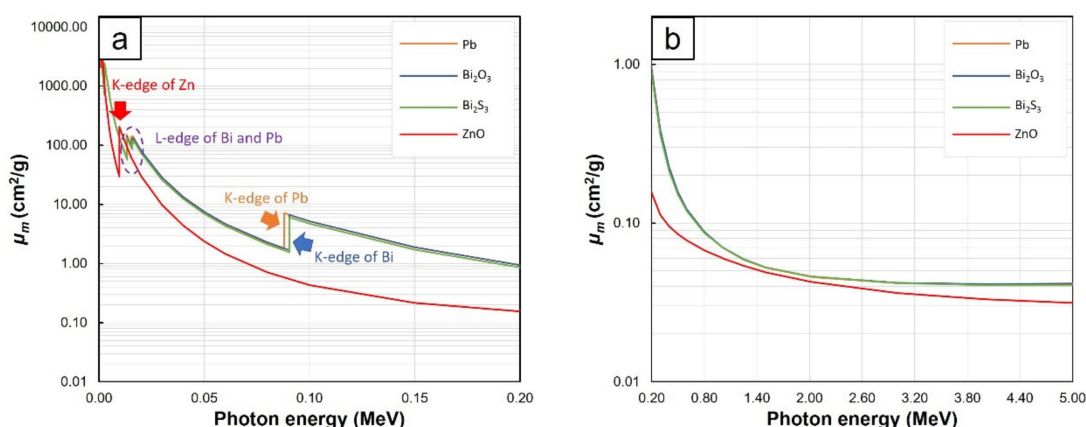
Figure 6. μ_m values of Pb, Bi_2O_3, Bi_2S_3, and ZnO, showing K-edge and L-edge behavior of Pb, Bi, and Zn at photon energies of (**a**) 0.001–0.2 MeV and (**b**) 0.2–5 MeV.

And in all composites at the photon energy of 9.6 keV (Figure 1a,c, Figure 2a,c, and Figure 3a,c) due to the K-edge of Zn atoms in ZnO (Figure 6). At these uncharacteristically high values of μ_m, the photon energies were just above the binding energy of the electron shells inside the atoms (the binding energy of the electrons at K-shell and L-shell were called K-edge and L-edge, respectively), resulting in substantially enhanced probabilities of photon interaction through photoelectric absorption at these particular energies [29]. It is noteworthy that values of μ_m in pristine NR were higher than those in Bi_2O_3/NR, Bi_2S_3, and Pb/NR at the photon energies of 1–2 MeV. These behaviors were due to the rapid drops in photoelectric absorption and Compton scattering probabilities of Bi_2O_3, Bi_2S_3, and Pb particles at these mid-ranged photon energies. These behaviors were in contrast with the decreases in interaction probabilities of C and H that were much less pronounced (μ_m of NR was actually higher than Bi_2O_3, Bi_2S_3, and Pb at these energy range). However, pair- production probability of Bi_2O_3, Bi_2S_3, and Pb sharply increases at photon energies greater than 2 MeV, resulting in much enhanced interaction probabilities of composites containing Bi_2O_3, Bi_2S_3, and Pb that consequently led to higher μ_m in Bi_2O_3/NR, Bi_2S_3/NR, and Pb/NR composites (pair production cross sections (probabilities) of light elements were relatively smaller than those of heavy elements).

Figure 4 also revealed that the Pb/NR composites generally had higher μ_m values than the Bi_2O_3/NR and Bi_2S_3/NR composites for the same filler content and photon energy (Figure 4a,b,d). This was due to the higher μ_m of Pb compared to Bi (Figure 6) and the dilution effect of O and S in Bi_2O_3 and Bi_2S_3, respectively that further reduced influences of Bi. However, the μ_m values of the Bi_2O_3/NR composites shown in Figure 4c were slightly higher than those of the Pb/NR composites at a photon energy of 1 MeV because, for this particular range of energies, Bi_2O_3 had slightly higher μ_m values than Pb (0.0713 and 0.0710 cm^2/g, respectively), resulting in higher attenuation abilities and consequently, higher μ_m values in the Bi_2O_3/NR composites. In addition, comparing μ_m values of NR and

wood/NR composites with the addition of Bi_2O_3 and Bi_2S_3 at the same filler content and photon energy, Figure 4 revealed that those with Bi_2O_3 exhibited slightly higher μ_m than those with Bi_2S_3. This could be due to higher mass fraction of Bi in a molecule of Bi_2O_3 (0.89) than Bi_2S_3 (0.81), which resulted in higher numbers of Bi atoms in Bi_2O_3 than Bi_2S_3 at the same filler content.

To validate the simulated results from XCOM in this work, previously reported experimental values were used to compare their agreements. The comparisons of the two values for the NR composites containing different filler types/contents at various photon energies are shown in Table 2. The percentage difference between the two values (Difference (%)) was calculated based on Equation (9):

$$\text{Difference (\%)} = \frac{\left| \mu_{m,XCOM} - \mu_{m,report} \right|}{\mu_{m,XCOM}} \times 100\% \tag{9}$$

where Difference (%) is the percentage of difference between simulated result from XCOM and the previously reported experimental value, $\mu_{m,XCOM}$ is the μ_m value from the simulated result, $\mu_{m,report}$ is the μ_m value from the previously reported experimental value.

As shown in Table 2, the range for Difference (%) was 0.0–17.9% with the average value being 5.3%. This comparison clearly showed that the simulated results from XCOM were in acceptable agreement with the experimental data; hence, they could be reliably used in later investigations of μ, *HVL*, and the recommended filler contents in this work. It should be pointed out that the differences in the two values could have been due to several factors, including experimental setup and equipment that caused an imperfectly monoenergetic and narrow photon beam, agglomerations of fillers, voids at the interfacial surfaces of the NR matrix and filler particles, and build-up factors that lowered the experimental μ_m values to be generally less than the theoretical ones [13,32].

3.2. Linear Attenuation Coefficients (μ) and Half Value Layer (HVL)

To determine the μ and *HVL* values of the Bi_2O_3/NR, Bi_2S_3/NR, Pb/NR, Bi_2O_3/wood/NR, Bi_2S_3/wood/NR, and Pb/wood/NR composites, the densities for each filler content must be estimated. The results of the density calculations using Equation 3 are shown in Table 3, which indicates that densities generally increased with increasing filler contents and the NR composites containing Pb had slightly higher densities than those with Bi_2O_3 and Bi_2S_3 due to the higher density of Pb (11.35 g/cm^3) compared to Bi_2O_3 (8.90 g/cm^3) and Bi_2S_3 (6.78 g/cm^3). Furthermore, Table 3 shows that the NR composites with the addition of wood particles had lower densities than those without wood particles (for the same filler content), mainly due to the much lower density of the wood particles (0.52 g/cm^3) compared to NR (0.92 g/cm^3), Bi_2O_3, Bi_2S_3, and Pb. It should be noted that the densities of actual NR and wood/NR composites might differ from the theoretical densities shown in Table 2 due to possible aggregation of fillers, poor interfacial compatibility between fillers and NR matrix, and incomplete vulcanization of NR from the obstruction of fillers during the curing process.

Table 2. Comparative μ_m values from simulated data using XCOM and previously reported experimental results of NR composites containing different filler types/contents at various photon energies.

Filler Type	Content (phr)	Photon Energy (MeV)	μ_m (cm^2/g)			Reference
			XCOM	Literature Value	Difference (%)	
Pb	0 40 80	0.122	0.162 0.943 1.459	0.159 0.813 1.198	1.9 13.8 17.9	[30]
Pb	0 40 80	0.356	0.108 0.149 0.176	0.106 0.142 0.166	1.9 4.7 5.7	[30]
Pb	0 40 80	0.662	0.084 0.090 0.094	0.086 0.089 0.091	2.4 1.1 3.2	[30]
Pb	100 300 500 1000	0.662	0.095 0.103 0.106 0.110	0.085 0.094 0.096 0.092	10.5 8.7 9.4 16.4	[22]
Pb	0 40 80	1.173	0.063 0.063 0.063	0.064 0.063 0.063	1.6 0.0 0.0	[30]
Pb	100 300 500 1000	1.250	0.060 0.060 0.059 0.059	0.051 0.052 0.056 0.051	15.0 13.3 5.1 13.6	[22]
Pb	0 40 80	1.332	0.059 0.059 0.059	0.059 0.058 0.058	0.0 1.7 1.7	[30]
Bi$_2$O$_3$	0 20 40 80 150	0.223	0.129 0.206 0.255 0.342 0.463	0.130 0.225 0.289 0.382 0.469	0.2 8.8 13.4 11.8 1.4	[31]
Bi$_2$O$_3$	0 20 40 80 150	0.253	0.124 0.183 0.220 0.286 0.379	0.123 0.190 0.237 0.304 0.371	0.8 3.8 7.7 6.3 2.1	[31]
Bi$_2$O$_3$	0 20 40 80 150	0.341	0.110 0.134 0.148 0.175 0.212	0.112 0.138 0.163 0.188 0.216	1.8 3.0 10.1 7.4 1.9	[31]
Bi$_2$O$_3$	0 20 40 80 150	0.482	0.095 0.104 0.109 0.119 0.132	0.096 0.106 0.116 0.124 0.137	1.1 1.9 6.4 4.2 3.8	[31]
Bi$_2$O$_3$	0 20 40 80 150	0.662	0.083 0.087 0.089 0.092 0.098	0.083 0.088 0.091 0.095 0.097	0.0 1.2 2.3 3.3 1.0	[31]

Table 3. Densities of Bi_2O_3/NR, Bi_2S_3/NR, Pb/NR, Bi_2O_3/wood/NR, Bi_2S_3/wood/NR, and Pb/wood/NR composites with filler contents varying from 0 to 1000 phr (in 40-phr increments), calculated using Equation (3).

Content (phr)	Density (g/cm^3)					
	Bi_2O_3/NR	Bi_2S_3/NR	Pb/NR	Bi_2O_3/Wood/NR	Bi_2S_3/Wood/NR	Pb/Wood/NR
0	1.09	1.08	1.08	0.96	0.95	0.95
40	1.36	1.33	1.36	1.17	1.15	1.17
80	1.61	1.56	1.61	1.37	1.34	1.37
120	1.84	1.77	1.86	1.56	1.51	1.57
160	2.05	1.96	2.09	1.74	1.67	1.76
200	2.26	2.14	2.32	1.91	1.83	1.94
240	2.45	2.31	2.53	2.07	1.97	2.12
280	2.63	2.46	2.73	2.22	2.11	2.29
320	2.80	2.61	2.92	2.37	2.23	2.45
360	2.97	2.74	3.11	2.51	2.36	2.61
400	3.12	2.87	3.28	2.65	2.47	2.76
440	3.27	2.99	3.45	2.78	2.58	2.91
480	3.41	3.10	3.62	2.90	2.68	3.05
520	3.54	3.21	3.77	3.02	2.78	3.19
560	3.67	3.30	3.92	3.14	2.88	3.32
600	3.79	3.40	4.06	3.25	2.97	3.45
640	3.90	3.49	4.20	3.36	3.05	3.57
680	4.01	3.57	4.34	3.46	3.14	3.69
720	4.12	3.65	4.46	3.56	3.20	3.81
760	4.22	3.73	4.59	3.65	3.29	3.92
800	4.31	3.80	4.71	3.74	3.36	4.03
840	4.41	3.87	4.82	3.83	3.43	4.14
880	4.50	3.94	4.93	3.92	3.50	4.24
920	4.58	4.00	5.04	4.00	3.56	4.34
960	4.66	4.06	5.15	4.08	3.62	4.44
1000	4.74	4.12	5.25	4.16	3.68	4.54

Figures 7 and 8 illustrate the values of μ and *HVL* of the Bi_2O_3/NR, Bi_2S_3/NR, Pb/NR, Bi_2O_3/wood/NR, Bi_2S_3/wood/NR, and Pb/wood/NR composites with varying filler contents and photon energies. The results indicated that μ tended to increase but *HVL* tended to decrease with increasing filler contents. These results agreed with the trends found in μ_m (Figures 1–4) due to the capability of Bi and Pb atoms to enhance the interaction probabilities between incident photons and the composites, leading to higher photon attenuation per unit length (μ), and consequently, less material thickness being required to attenuate 50% of the incident photon intensity (*HVL*). Additionally, Figure 7 shows that the Pb/NR composites had relatively higher μ values than the Bi_2O_3/NR composites for the same filler content and photon energy, mainly due to the former having greater density and μ_m than the latter (Equation (1)). Similarly, the NR composites with the addition of wood particles had lower μ but higher *HVL* values than those without wood particles. This behavior was observed due to the low density of the wood particles (Table 1) that generally decreased the density of the NR composites (Table 3) as well as the relatively low μ_m of wood particles compared to Bi_2O_3, Bi_2S_3, and Pb. Nonetheless, although the shielding properties of the NR composites containing Bi_2O_3 (Bi_2S_3) were reduced by as much as 16% (33%) at a photon energy of 0.1 MeV and by 5% (24%) at a photon energy of 5 MeV (determined at 1000 phr, which was the highest content investigated in this work), the potential of using bismuth compounds, especially Bi_2O_3, as an alternative but safer protective filler was promising. In addition, the μ (*HVL*) values at lower energies were generally higher (lower) than those at higher energies and the effects of additional filler contents on enhancing shielding abilities were more pronounced at lower energies than at higher energies (determined for the same type of composites). This could have been due to the higher-energy photons being less likely to interact with the materials they

encountered (Equations (6)–(8)), leading to less attenuation and therefore, smaller (larger) μ (*HVL*) values.

3.3. Recommended Contents of Bi_2O_3, Bi_2S_3, and Pb in NR and Wood/NR Composites

To determine the recommended filler contents for the Bi_2O_3/NR, Bi_2S_3/NR, Pb/NR, Bi_2O_3/wood/NR, Bi_2S_3/wood/NR, and Pb/wood/NR composites at different photon energies, the values of *%change* in μ were calculated using Equation 4 and the results are shown in Figure 9. The results indicated that the recommended contents for Bi_2O_3, Bi_2S_3, and Pb were in the ranges 358–594 phr, 316–557 phr, and 398–624 phr, respectively, depending on photon energies and the present of wood particles. Furthermore, it is noteworthy that values of *%change* were initially much higher at low filler contents due to the more pronounced effects of Bi and Pb in enhancing shielding properties from their relatively higher cross sections for photoelectric absorption and Compton scattering than C, H, and O in the pristine NR and wood/NR composites. This effect led to a significant enhancement in photon attenuation of the NR composites at low photon energies. However, as more fillers were added to the composites, the effects of fillers on *%change* were less pronounced and essentially became less than 5% (a threshold set in this work for the determination of recommended filler contents).
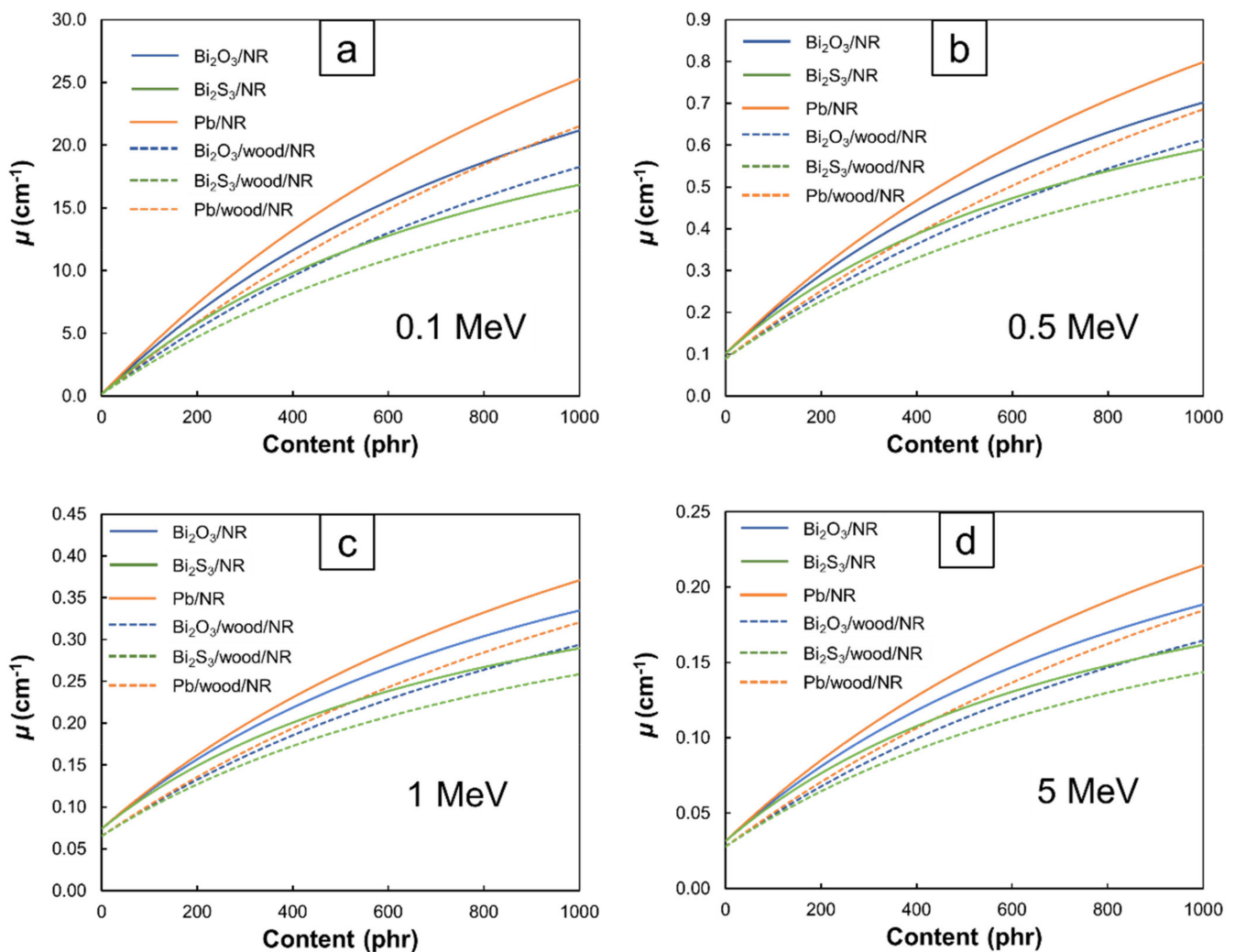
Figure 7. μ values of Bi_2O_3/NR, Bi_2S_3/NR, Pb/NR, Bi_2O_3/wood/NR, Bi_2S_3/wood/NR, and Pb/wood/NR composites at photon energies of (**a**) 0.1 MeV, (**b**) 0.5 MeV, (**c**) 1 MeV, and (**d**) 5 MeV.
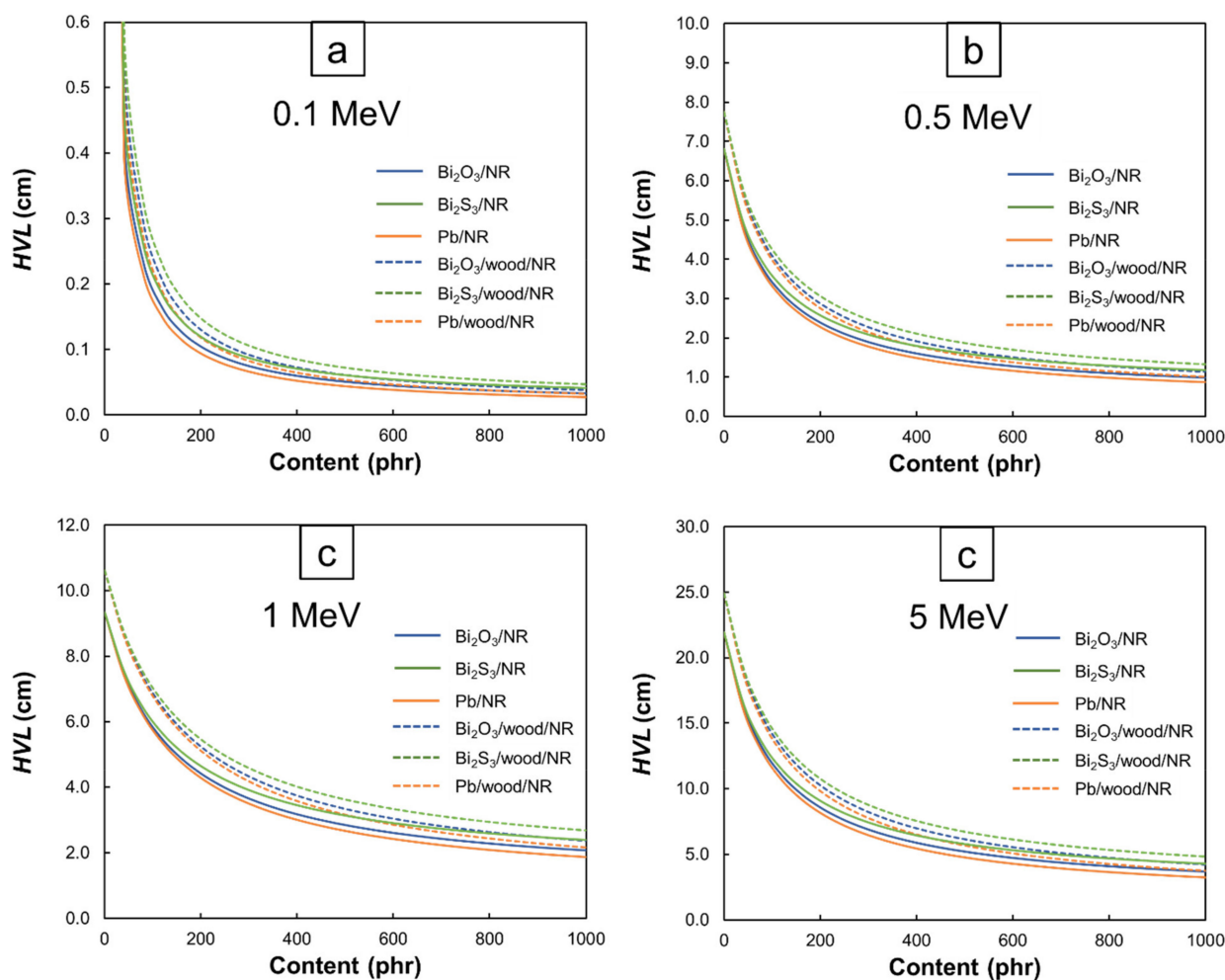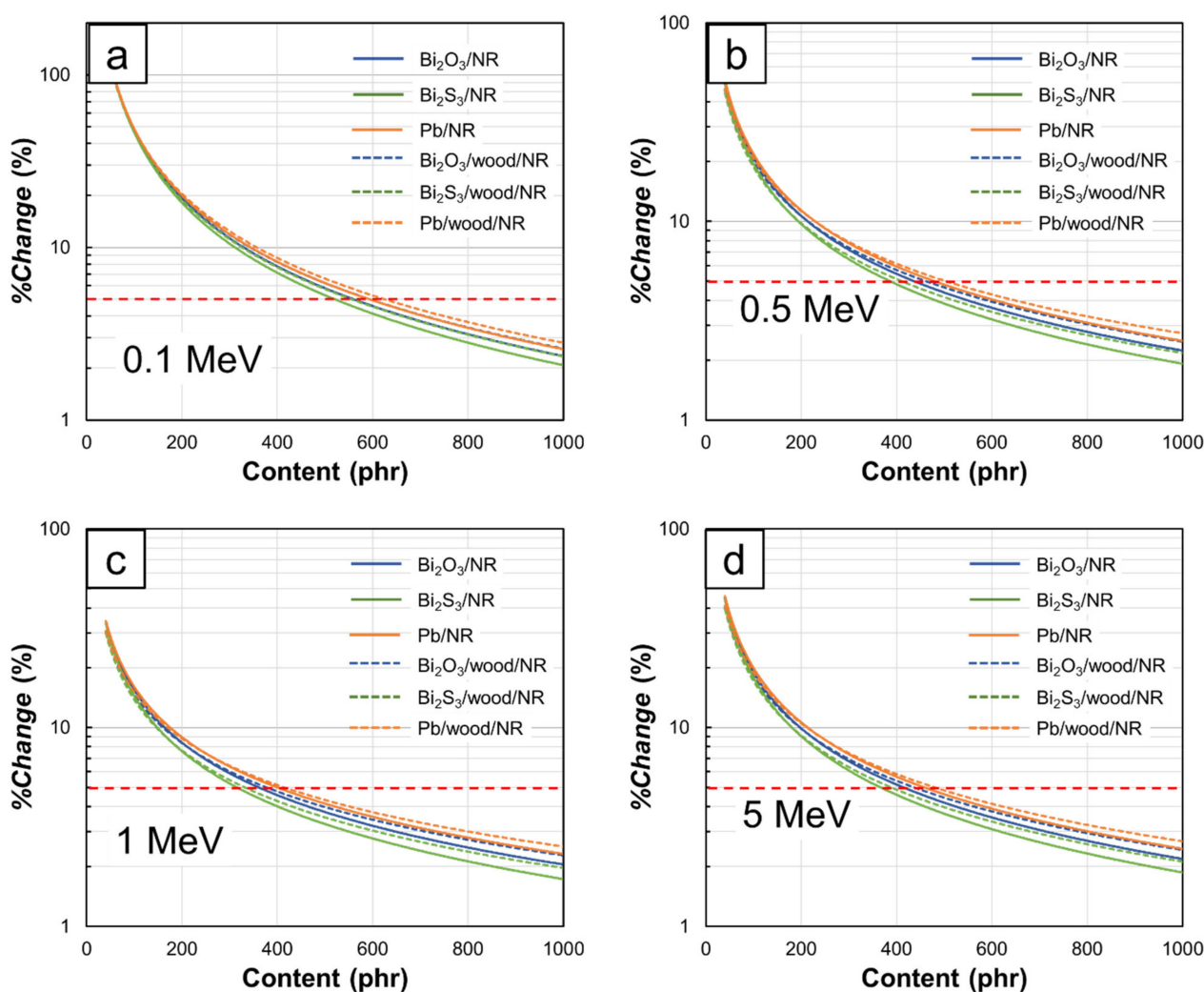
Figure 8. *HVL* values of Bi$_2$O$_3$/NR, Bi$_2$S$_3$/NR, Pb/NR, Bi$_2$O$_3$/wood/NR, Bi$_2$S$_3$/wood/NR, and Pb/wood/NR composites at photon energies of (**a**) 0.1 MeV, (**b**) 0.5 MeV, (**c**) 1 MeV, and (**d**) 5 MeV.

To obtain the recommended filler contents for all photon energies, fitted curves of *%change* with the form shown in Equation (5) were developed and mathematical constants (A and B) were obtained using a trendline function available in Microsoft Excel. The values of A and B as well as recommended filler contents for photon energies of 0.1 MeV, 0.5 MeV, 1 MeV, and 5 MeV (based on the threshold of 5%) determined from the fitted curves are shown in Table 4, which indicated that lower photon energies (0.1 MeV and 0.5 MeV) required higher filler contents to achieve less than 5% of *%change* than those at higher photon energies (1 MeV and 5 MeV). This behavior was observed because Bi$_2$O$_3$, Bi$_2$S$_3$, and Pb could better interact with photons at lower energies, leading to greater shielding enhancement after adding more fillers to the composites.

Table 4 also shows the effects of potentially replacing Pb with Bi$_2$O$_3$ or Bi$_2$S$_3$ by considering the percentage difference in μ values of Pb and Bi$_2$O$_3$ (Bi$_2$S$_3$) at the determined recommended contents. The results indicated that the differences were in the range 8.3–16.3% for those with Bi$_2$O$_3$ and 19.6–28.4% for those with Bi$_2$S$_3$, of which NR and wood/NR composites containing Pb had higher μ values than those with Bi$_2$O$_3$ and Bi$_2$S$_3$. Nonetheless, as a considerably safer chemical than Pb, bismuth compounds, especially Bi$_2$O$_3$, showed their potential to replace the former as effective radiation-protective fillers.

Interestingly, Table 4 reveals that the recommended filler contents for 1 MeV photons were the lowest among all energies. This could be explained using Figure 4c, which indicates that the μ_m values for all filler contents were not greatly different (0.068–0.071 cm^2/g), resulting in lower filler contents being required to obtain <5% of *%change*. On the other hand, the results pointed out that higher filler contents were required to achieve the same *%change* at the 5 MeV photon energy, mostly due to the initiation of pair production, which again enhanced the effects of added Bi$_2$O$_3$, Bi$_2$S$_3$, and Pb in photon attenuation, as seen by larger changes in μ_m when the filler contents increased from 0 to 1000 phr (μ_m increased from 0.029 to 0.040 cm^2/g). It should be noted that the recommended filler contents given in this work were not intended for the highest μ of the composites but rather the least amount of filler that produced a *%change* of an additional 40 phr filler to be less than 5% in order to minimize the effects of having too much filler in the NR matrix and its impact on lowering mechanical properties [13,20,24,31].

Figure 9. *%change* in μ values at photon energies of (**a**) 0.1 MeV, (**b**) 0.5 MeV, (**c**) 1 MeV, and (**d**) 5 MeV after addition of 40-phr Bi$_2$O$_3$, Bi$_2$S$_3$, or Pb into Bi$_2$O$_3$/NR, Bi$_2$S$_3$/NR, Pb/NR, Bi$_2$O$_3$/wood/NR, Bi$_2$S$_3$/wood/NR, and Pb/wood/NR composites. Horizontal dotted lines represent the threshold set in this work to determine recommended filler contents (*%change* < 5%).

Table 4. Mathematical constants from Figure 9, recommended filler contents at photon energy of 0.1–5 MeV (*%change* < 5%), and percentage of difference between NR (wood/NR) composites containing Bi_2O_3, Bi_2S_3, and Pb.

Composite	Photon Energy (MeV)	Coefficient		Recommended Content (phr)	μ at Recommended Content (cm^{-1})	Percentage Difference from Composites with Pb (%) *
		A	B			
Pb/NR	0.1	1.652×10^4	−1.269	593	17.8	n/a **
	0.5	1.664×10^3	−0.941	478	0.52	n/a
	1	760.3	−0.839	398	0.23	n/a
	5	1.312×10^3	−0.909	458	0.14	n/a
Bi_2O_3/NR	0.1	1.894×10^4	−1.303	557	14.9	16.3
	0.5	1.839×10^3	−0.972	436	0.46	11.5
	1	869.4	−0.877	358	0.21	8.7
	5	1.439×10^3	−0.940	413	0.12	14.3
Bi_2S_3/NR	0.1	2.271×10^4	−1.346	521	12.8	28.4
	0.5	2.011×10^3	−1.007	386	0.39	24.6
	1	985.0	−0.918	316	0.18	20.1
	5	1.623×10^3	−0.980	365	0.11	24.8
Pb/wood/NR	0.1	1.389×10^4	−1.232	624	15.3	n/a
	0.5	1.199×10^3	−0.881	502	0.44	n/a
	1	535.9	−0.776	413	0.20	n/a
	5	0.937×10^3	−0.848	476	0.12	n/a
Bi_2O_3/wood/NR	0.1	1.553×10^4	−1.259	594	12.8	16.3
	0.5	1.303×10^3	−0.907	461	0.40	9.1
	1	600.5	−0.808	375	0.18	10.0
	5	1.008×10^3	−0.874	434	0.11	8.3
Bi_2S_3/wood/NR	0.1	1.812×10^4	−1.297	557	11.2	26.6
	0.5	1.402×10^3	−0.937	410	0.35	21.5
	1	670.5	−0.844	332	0.16	19.6
	5	1.121×10^3	−0.908	388	0.09	22.1

* Determined with respect to Pb/NR or Pb/wood/NR composites at the same photon energy. ** n/a: not applicable.

4. Conclusions

This work determined the theoretical high-energy photon shielding properties consisting of μ_m, μ, and *HVL* as well as the recommended filler contents for Bi_2O_3/NR, Bi_2S_3/NR, Pb/NR, Bi_2O_3/wood/NR, Bi_2S_3/wood/NR, and Pb/wood/NR composites with the filler contents in the range 0–1000 phr and photon energies in the range 0.001–5 MeV for the development of X-ray and gamma-shielding equipment with flexibility and enhanced dimensional stability. The XCOM simulation software was used in this work and was provided by NIST, USA. The results showed that values of μ_m and μ (*HVL*) increased (decreased) with increasing filler contents but decreased (increased) with increasing photon energies. Furthermore, the addition of wood particles in the wood/NR composites did not greatly affect the overall shielding properties compared with the NR composites, implying the possibility of applying wood fillers as a dimensional reinforcer for composites with high filler contents. In addition, Bi_2O_3 and Bi_2S_3 also showed great potential to replace Pb as a high-energy-photon protective filler due to its relatively high attenuation efficiency and being considerably less hazardous than Pb. Lastly, the determination of the recommended filler contents based on calculation of the *%change* in μ indicated that the optimum Pb, Bi_2O_3, or Bi_2S_3 contents at photon energies of 0.1, 0.5, 1, and 5 MeV were in the range 316–624 phr, depending on the filler type and the intended photon energy.

composites, Table S10: Mass attenuation coefficients (μ_m) of 800-phr-Bi_2O_3/wood/NR composites, Table S11: Mass attenuation coefficients (μ_m) of 400-phr-Pb/wood/NR composites, Table S12: Mass attenuation coefficients (μ_m) of 800-phr-Pb/wood/NR composites, Table S13: Mass attenuation coefficients (μ_m) of 400-phr-Bi_2S_3/wood/NR composites, Table S14: Mass attenuation coefficients (μ_m) of 800-phr-Bi_2S_3/wood/NR composites.

Conflicts of Interest: The authors declare no conflict of interest. The funders had no role in the design of the study; in the collection, analyses, or interpretation of data; in the writing of the manuscript, or in the decision to publish the results.

References

1. Sakdinawat, A.; Attwood, D. Nanoscale X-ray imaging. *Nat. Photon.* **2010**, *4*, 840–848. [CrossRef]
2. Zhao, C.; Fezzaa, K.; Cunningham, R.W.; Wen, H.; De Carlo, F.; Chen, L.; Rollett, A.D.; Sun, T. Real-time monitoring of laser powder bed fusion process using high-speed X-ray imaging and diffraction. *Sci. Rep.* **2017**, *7*, 3602. [CrossRef] [PubMed]
3. Smeets, J.; Roellinghoff, F.; Prieels, D.; Stichelbaut, F.; Benilov, A.; Busca, P.; Fiorini, C.; Peloso, R.; Basilavecchia, M.; Frizzi, T.; et al. Prompt gamma imaging with a slit camera for real-time range control in proton therapy. *Phys. Med. Biol.* **2012**, *57*, 3371–3405. [CrossRef] [PubMed]
4. Fan, F.; Gao, S.; Ji, S.; Fu, Y.; Zhang, P.; Xu, H. Gamma radiation-responsive side-chain tellurium-containing polymer for cancer therapy. *Mater. Chem. Front.* **2018**, *2*, 2109–2115. [CrossRef]
5. Shin, J.M.; Kim, B.K.; Seol, S.G.; Jeon, S.B.; Kim, J.S.; Jun, B.K.; Kang, S.Y.; Lee, J.S.; Chung, M.N.; Kim, S.H. Mutation breeding of sweet potato by gamma-ray radiation. *Afr. J. Agric. Res.* **2011**, *6*, 1447–1454.
6. El-Taher, A. Elemental analysis of granite by instrumental neutron activation analysis (INAA) and X-ray fluorescence analysis (XRF). *Appl. Radiat. Isot.* **2012**, *70*, 350–354. [CrossRef] [PubMed]
7. Rybkina, V.L.; Bannikova, M.; Adamova, G.V.; Dorr, H.; Scherthan, H.; Azizova, T.V. Immunological markers of chronic occupational radiation exposure. *Health Phys.* **2018**, *115*, 108–113. [CrossRef] [PubMed]
8. Luckey, T.D. Biological effects of ionizing radiation: A perspective for Japan. *J. Am. Physicians Surg.* **2011**, *16*, 45–46.
9. Garau, M.M.; Calduch, A.L.; Lopez, E.C. Radiobiology of the acute radiation syndrome. *Rep. Pract. Oncol. Radiother.* **2011**, *16*, 123–130. [CrossRef]
10. Tiamduangtawan, P.; Kamkaew, C.; Kuntonwatchara, S.; Wimolmala, E.; Saenboonruang, K. Comparative mechanical, self-healing, and gamma attenuation properties of PVA hydrogels containing either nano- or micro-sized Bi_2O_3 for use as gamma-shielding materials. *Radiat. Phys. Chem.* **2020**, *177*, 109164. [CrossRef]
11. McGiff, T.J.; Danforth, R.A.; Herschaft, E.E. Maintaining radiation exposures as low as reasonably achievable (ALARA) for dental personnel operating portable hand-held X-ray equipment. *Health Phys.* **2012**, *103*, S179–S185. [CrossRef] [PubMed]
12. Bouffler, S.; Ainsbury, E.; Gilvin, P.; Harrison, J. Radiation-induced cataracts: The Health Protection Agency's response to the ICRP statement on tissue reactions and recommendation on the dose limit for the eye lens. *J. Radiol. Prot.* **2012**, *32*, 479–488. [CrossRef]
13. Poltabtim, W.; Wimolmala, E.; Saenboonruang, K. Properties of lead-free gamma-ray shielding materials from metal oxide/EPDM rubber composites. *Radiat. Phys. Chem.* **2018**, *153*, 1–5. [CrossRef]
14. Toyen, D.; Rittirong, A.; Poltabtim, W.; Saenboonruang, K. Flexible, lead-free, gamma-shielding materials based on natural rubber/metal oxide composites. *Iranian Polym. J.* **2018**, *27*, 33–41. [CrossRef]
15. Hashemi, S.A.; Mousavi, S.M.; Gaghihi, R.; Arjmand, M.; Rahsepar, M.; Bahrani, S.; Ramakrishna, S.; Lai, C.W. Superior X-ray radiation shielding effectiveness of biocompatible polyaniline reinforced with hybrid graphene oxide-iron tungsten nitride flakes. *Polymers* **2020**, *12*, 1407. [CrossRef] [PubMed]
16. Yao, Y.; Zhang, X.; Li, M.; Yang, R.; Jiang, T.; Lv, J. Investigation of gamma ray shielding efficiency and mechanical performances of concrete shields containing bismuth oxide as an environmentally friendly additive. *Radiat. Phys. Chem.* **2016**, *127*, 188–193. [CrossRef]
17. Low, D.Y.S.; Supramaniam, J.; Soottitantawat, A.; Charinpanitkul, T.; Tanthapanichakoon, W.; Tan, K.W.; Tang, S.Y. Recent developments in nanocellulose-reinforced rubber matrix composites: A review. *Polymers* **2020**, *13*, 550. [CrossRef] [PubMed]

18. Azeez, A.B.; Mohammed, K.S.; Abdullah, M.M.A.B.; Zulkepli, N.N.; Sandu, A.V.; Hussin, K.; Rahmat, A. Design of flexible green anti-radiation shielding material against gamma-ray. *Mater. Plast.* **2014**, *51*, 300–308.
19. Salimi, M.; Ghal-Eh, N.; Amirabadi, E.A. Characterization of a new shielding rubber for use in neutron–gamma mixed fields. *Nucl. Sci. Tech.* **2018**, *29*, 36. [CrossRef]
20. Ninyong, K.; Wimolmala, E.; Sombatsompop, N.; Saenboonruang, K. Properties of natural rubber (NR) and wood/NR composites as gamma shielding materials. *IOP Conf. Ser. Mater. Sci. Eng.* **2019**, *526*, 012038. [CrossRef]
21. Flora, G.; Gupta, D.; Tiwari, A. Toxicity of lead: A review with recent updates. *Interdiscip. Toxicol.* **2012**, *5*, 47–58. [CrossRef] [PubMed]
22. Gwaily, S.E.; Madani, M.; Hassan, H.H. Lead-Natural rubber composites as gamma radiation shields. II: High concentration. *Polym. Compos.* **2012**, *23*, 495–499. [CrossRef]
23. Ozdemir, T.; Gungor, A.; Reyhancan, I.A. Flexible neutron shielding composite material of EPDM rubber with boron trioxide: Mechanical, thermal investigations and neutron shielding tests. *Radiat. Phys. Chem.* **2017**, *131*, 7–12. [CrossRef]
24. Ninyong, K.; Wimolmala, E.; Sombatsompop, N.; Saenboonruang, K. Potential use of NR and wood/NR composites as thermal neutron shielding materials. *Polym. Test.* **2017**, *59*, 336–343. [CrossRef]
25. Berger, M.J.; Hubbell, J.H.; Seltzer, S.M.; Chang, J.; Coursey, J.S.; Sukumar, R.; Zucker, D.S.; Olsen, K. *XCOM: Photon Cross Section Database (Version 1.5)*; National Institute of Standards and Technology: Gaithersburg, MD, USA, 2010. Available online: http://physics.nist.gov/xcom (accessed on 30 January 2021).
26. Livet, F.; Sutton, M. X-ray coherent scattering in metal physics. *C. R. Phys.* **2012**, *13*, 227–236. [CrossRef]
27. Hirayama, H. Lecture Note on Photon Interactions and Cross Sections. Available online: http://rcwww.kek.jp/research/shield/photon_r.pdf (accessed on 1 February 2021).
28. Bruce, W.B.; Pearson, M.L.; Freedhoff, H.S. The linear energy transfer distributions resulting from primary and scattered X-rays and gamma rays with primary HVL's from 1.25 mm Cu to 11 mm Pb. *Radiat. Res.* **1963**, *19*, 606–620. [CrossRef]
29. Si-Mohamed, S.; Cormode, D.P.; Bar-Ness, D.; Sigovan, M.; Naha, P.C.; Langlois, J.B.; Chalabreysse, L.; Coulon, P.; Blevis, I.; Roessl, E.; et al. Evaluation of spectral photon counting computed tomography K-edge imaging for determination of gold nanoparticle biodistribution in vivo. *Nanoscale* **2017**, *46*, 18246–18257. [CrossRef] [PubMed]
30. El-Khatib, A.M.; Doma, A.S.; Badawi, M.S.; Abu-Rayan, A.E.; Aly, N.S.; Alzahrani, J.S.; Abbas, M.I. Conductive natural and waste rubbers composites-loaded with lead powder as environmental flexible gamma radiation shielding material. *Mater. Res. Express* **2020**, *7*, 105309. [CrossRef]
31. Intom, S.; Kalkornsurapranee, E.; Johns, J.; Kaewjaeng, S.; Kothan, S.; Hongtong, W.; Chaiphaksa, W.; Kaewkhao, J. Mechanical and radiation shielding properties of flexible material based on natural rubber/ Bi_2O_3 composites. *Radiat. Phys. Chem.* **2020**, *172*, 108772. [CrossRef]
32. Obaid, S.S.; Sayyed, M.I.; Gaikwad, D.K.; Pawar, P.P. Attenuation coefficients and exposure buildup factor of some rocks for gamma ray shielding applications. *Radiat. Phys. Chem.* **2018**, *148*, 86–94. [CrossRef]